Proc. VIIth Digital Image Computing: Techniques and Applications, Sun C., Talbot H., Ourselin S. and Adriaansen T. (Eds.), 10-12 Dec. 2003, Sydney

Accurate Curvilinear Modelling for Precise Measurements of Tubular Structures

Rongxin Li and Sébastien Ourselin

BioMedIA Lab
CSIRO ICT Centre
Cnr Vimiera & Pembroke Rd, Marsfield NSW 2122, Australia
Ron.Li@CSIRO.au
http://www.tip.csiro.au

Abstract. Accurate curvilinear models of tubular structures are essential for the precise measurements and description of those structures. Two major obstacles to obtaining an accurate curvilinear model from a three-dimensional (3D) image are tortuosity of the tubular structure and interferences from such sources as foreign entities in the neighborhood, pathological deformation and artifacts. Using existing algorithms, the tortuosity and interferences can give rise to models that tend to significantly distort subsequent length and angle measurements. In this paper, we describe a novel approach that overcomes those obstacles by combining a knowledge-embedding model with a front propagation method. We then demonstrate the effectiveness of our method through its potential applications in path planning and measurement for minimally invasive diagnosis and treatment purposes.

1 Introduction

Precise measurements and description of tubular structures play critical roles in a variety of situations. In the medical domain, for example, such measurements and description are often pre-requisites for minimally invasive diagnostic or therapeutic procedures (e.g. [4]). Traditionally, unless direct, invasive and even potentially morbid measurement techniques (e.g. aortic and iliac digital subtraction angiography, which carries the risk of haemorrhage, false aneurysm and dissection) are used, significant expertise, experience and effort are required in order to overcome limitations in the images (e.g. elongated structures running oblique to the slicing plane) and discount potentially interfering factors (e.g. variation of the width). With computerized assistance, it is possible to reliably achieve a high level of accuracy with significantly less effort. For example, it is possible to abstract away potentially interfering details and retain only the essential geometry relevant to the planning by constructing a curvilinear model of the tubular structure, and to conduct automatic length, angle and tortuosity measurements based on this model.

Despite those advantages, existing computer-based approaches are not able to consistently meet high accuracy requirements. Two main types of challenges

are tortuosity of the tubular structure, and interferences from sources such as foreign entities in the neighbourhood, pathological deformation and artifacts. Using existing algorithms, the tortuosity and interferences can give rise to undesirable models that tend to significantly distort subsequent measurements. In contrast, our new approach is able to satisfactorily deal with both situations. In this paper, we describe this approach and demonstrate its efficacy through its potential applications in path planning and measurement for minimally invasive diagnosis and treatment purposes.

This paper is organized as follows. We review the relevant literature in Section 2, and detail the key steps of our new algorithm in Section 3. In Section 4, we demonstrate the accuracy of our approach using Computed Tomography (CT) of the iliac artery, Magnetic Resonance Angiography (MRA) of the brain, and synthetic datasets.

2 Brief review of related methods

We define an accurate curvilinear model (ACM) of a tubular entity as an abstraction of the entity that is optimal for length, angle and tortuosity measurements. That is, it faithfully retains the geometric properties that are essential to those measurements, while excluding all potentially interfering details, such as width, width variation and branching.

Existing methods related to curvilinear modelling include the skeletonisation technique [15, 23], scale-space filtering and ridge traversal approaches (e.g. [10, 17, 11, 2], direct tracking [22, 12] and the Minimal Cost Path (MCP) approach. Among these, the MCP approach has certain distinct advantages, such as that it is robust to conditions like vessel stenosis, partial volume effects and noise. The MCP approach has traditionally been implemented using graph-search principles (e.g. [9]), but more recently simulated front propagation has emerged as a more favourable scheme due to its efficiency and ability to give sub-grid accuracy.

The main drawback of the MCP approach is that it tends to discourage curvature, which results in significant inaccuracies where the local curvature of the target structure is high. A recent approach proposed by Deschamps *et al* introduces a technique of using multiple passes of the Fast Marching Method to centre the resultant path [8, 21]. This technique corrects the inherent tendency of MCP algorithms to take shortcuts by largely constraining the MCP to travel on local maxima of the distances to the background. However, like the other approaches mentioned above, it is prone to introducing artificial tortuosity under certain circumstances, due to distortions of the ridge (composed of local maxima) in the distance map. For example, such distortions can occur if the target vessel has stenosis, or is compressed due to another structure touching it. Another example is that if the cross sections of a tubular structure are not perfectly round, pathological deformation (e.g. aneurysms) or foreign entities present in its neighbourhood can also distort the ridge.

While it is possible to smooth the track by adding a relatively large constant into the cost integral as suggested by Deschamps *et al* [8], such smoothing tends

to cancel out the work performed by the path centering technique, especially at high curvature positions. This is a dilemma that can be summarised in the following way: a non-centered path tends to take short cuts within the tubular wherever possible, but path centering can introduce artificial tortuosity. It is our belief that only through the use of *a priori* knowledge can this issue be satisfactorily resolved.

3 Method Description

3.1 Overview

The approach presented here for accurate curvilinear modeling uses both front propagation and *a priori* shape knowledge, with the latter embedded in a deformable model. To obtain suitable propagation channels, distances to the background are calculated and uniformly thresholded. Front propagation is then simulated from a start point using the Fast Marching Method to construct a map of propagation. A subsequent backtracking step from the end point using steepest descent generates the MCP.

At each point on the MCP, we resample the original data in planes perpendicular to the local orientation of the MCP. A deformable tubular model is then constructed inside the resampled data and allowed to evolve. At the end, the spine of the tubular model is extracted and transformed back into the coordinates of the original data. Through this process symmetric changes, such as sharp turns, are retained while many asymmetric changes, such as a branching event or aneurysms, are removed to a large extent. In addition, deforming the model in the transformed data domain markedly simplifies the computation.

We explain in detail the key steps of the algorithm in Section 3.2 and Section 3.3.

3.2 Front Propagation

Like the approach proposed by Deschamps *et al* [8], the initial stages of our method also involves computing a distance map and an MCP. However, we have chosen to use a more advantageous scheme. First, we use a chamfer algorithm [13, 3] to perform a distance transform (to the background) based on a thresholded image of the original. Being essentially mask operations, the chamfer technique is both efficient and simple. Although the resultant distances are not precisely Euclidean, the discrepancies do not affect our results. This is because only the order of distances, rather than the distance values *per se*, are of interest to our method. Using any of the common chamfer matrices (e.g. Borgefors', Verwer's and Kiryati's) this order is preserved on any imaginable size of grids for medical images.

After the end points are selected, the distance map is thresholded if the maximum distance values in corresponding connected components exceed a target value. Unlike its usage in other approaches (e.g. path centering, direct extraction

of the centerline through topology-preserving thinning), a distance transform is incorporated in our method for two reasons. Firstly, it helps the tubular model in the next stage to remain faithful to the structure of interest, especially at high curvature places of the structure, and promotes faster convergence of the deformation of the model. This is because better initialisation for the tubular model can be achieved with narrower propagation channels and with those channels well inside the structure of interest. Secondly, higher efficiency can be achieved by restricting the propagation area and, more importantly, by limiting "propagation leakage" through the reduction of the extent of branching and neighborhood touching.

Next, a propagation map is constructed, which is composed of arrivals times of the propagating wavefront. The problem is posed as:

$$|\nabla T|\, F = 1, \tag{1}$$

where T is the arrival time, and the speed F is defined as:

$$F = \frac{G_\sigma * I}{\max(G_\sigma * I)} + \alpha,$$

where I is the thresholded distance field, G_σ is a Gaussian kernel and α is a very small constant.

Equation (1) is the stationary case of the Hamilton-Jacobi equations, known as Eikonal equation. Based on the Hyperbolic Conservation Laws, Sethian ([1, 18, 19]) developed numerical methods to this formulation, known as the Fast Marching Method (FMM). The field of arrival times, or the propagation map, is iteratively updated by solving a discretized version of Equation (1). A high level of efficiency can be achieved by both using a binary heap data structure and restricting the computation of times to within a narrow band.

Although FMM is both efficient and can give sub-grid accuracy, it is perhaps worth noting that the link between the minimal cost path and wave propagation can be exploited with methods that model wave propagation in other ways. An example of this is a discrete state simulation of wave propagation, proposed in a recent paper by Quek and Kirbas [16].

3.3 Tubular shape model and transformed image domain

One commonality among vessels, ducts, bronchi and the colon are that they have circular or elliptical cross sections and smoothly varying radii [2]. To exploit this fact, a tubular shape model is used as a vehicle to carry knowledge about the desired structure for the purpose of filtering out any irrelevant bumps, branches or foreign objects in the neighbourhood. The knowledge is embedded not only in the mesh structure, but also in the internal forces of the model. The combination of the model's intra-ring forces (explained below) and the inflation force alone favours such an outcome that each cross-sectional ring of the resultant tubular model has a nearly constant area. Although the inter-ring forces help enforce this, in the present application they only play a secondary role. The internal forces can be designed so that the constant area favoured by the model approximately

corresponds to that of the structure being modeled. The use of a deflation force (see below) near the end of the deformation provides further assurance. The image force localizes the model.

A feature that makes our model simple and computationally efficient is that the model's deformation takes place in a transformed image. As mentioned above, the original data are resampled in planes perpendicular to the local orientation of the MCP. The resampled data are then stacked up to form a new, transformed data volume. An initial thin tube is constructed in the middle of the new data and allowed to evolve to minimize the following "energy" functional E of the model in a space of permissible deformations [20, 7]:

$$E(v) = \int_{\Omega} w_{10} \left|\frac{\partial v}{\partial s}\right|^2 + w_{01} \left|\frac{\partial v}{\partial r}\right|^2 + w_{11} \left|\frac{\partial^2 v}{\partial s \partial r}\right|^2 + w_{20} \left|\frac{\partial^2 v}{\partial s^2}\right|^2 + w_{02} \left|\frac{\partial^2 v}{\partial r^2}\right|^2 + P[v(s,r)]\, dsdr \quad (2)$$

where v(s, r) = (x(s, r), y(s, r), z(s, r)) is a parametric surface on a parameter region Ω, s and r are the parameterisation in the cross-sectional-tangential and axial directions respectively, $P(v)$ is the potential associated with external forces and can be defined as -$|\nabla I(v)|$, where I is the image. w_{10}, w_{01}, w_{11}, w_{20}, w_{02} control surface properties of tension, rigidity and resistance to twist (they are not necessarily constants). Used in our model, the coefficients w_{10} and w_{20} encode the strengths of the intra-ring forces mentioned above, while w_{01} and w_{02} represent those of the inter-ring forces. w_{11} is associated with a combination of intra and inter-ring forces. An inflation force is also used throughout the process.

A minimum of E can be reached by solving the associated Euler-Lagrange equation [14, 6]

$$\begin{aligned} &-\tfrac{\partial}{\partial s}\left(w_{10}\tfrac{\partial v}{\partial s}\right) - \tfrac{\partial}{\partial r}\left(w_{01}\tfrac{\partial v}{\partial r}\right) \\ &+2\tfrac{\partial^2}{\partial s \partial r}\left(w_{11}\tfrac{\partial^2 v}{\partial s \partial r}\right) + \tfrac{\partial^2}{\partial s^2}\left(w_{20}\tfrac{\partial^2 v}{\partial s^2}\right) \\ &+\tfrac{\partial^2 v}{\partial r^2}\left(w_{02}\tfrac{\partial^2 v}{\partial r^2}\right) + \nabla P(v) = 0 \end{aligned}$$

A numerical solution can be obtained using an evolution process by iteratively solving and updating a group of linear equations after a dynamic system corresponding to the above equation is discretized in both time and space [7, 6].

As has been well understood, the quality of the initialisation is critical to the success of an active surface model. In order to improve the initialisation at places of significant curvature, the evolution process is repeated after the model converges at a local energy minimum. In each repetition the resultant surface from the previous round is used for the initialisation. Three times of repetition is apparently adequate. However, this is subject to further experimental investigation. For the initialisation in the two repetitions before the last round, in the current implementation a simple shrinking operation is applied to the model.

In the final repetition of the iterative deformation, the resultant surface from the previous round is not shrunken prior to the initialisation, but an adaptive deflation force is used. Similar to the adaptivity proposed in other research (e.g.

[5]), the strength of this force is inversely related to the magnitude of the local gradient. In addition to the area targeting mentioned above, this force is employed to avoid the need to use strong forces in the axial direction of the tube in situations where gradients are sometimes deficient because of a nearby, touching object, such as a thrombus or a passing vessel.

Finally, the medial axis is transformed back to the coordinate system of the original data to form the ACM.

4 Results

Accurate knowledge of tubular entities is often crucial to the assessment and planning of minimally invasive surgery. Using clinical data, we demonstrate that our approach can produce ACMs in two types of surgery planning situations, respectively representing the two opposite aspects of the dilemma mentioned in Section 2. To clearly illustrate those situations and our solutions, however, we show two synthetic datasets first.

4.1 Synthetic Data

Our approach is applied to a situation where there is significant potential interference in the neighbourhood of a tubular structure. Two synthetic structures, a straight cylinder and a tortuous one, are used, as shown in Figure 1. Note that the elliptical shape of the cross-sections (as depicted in Figure 1) make it less resistant to outside interference. Our results, specifically the ACMs shown inside the 3D visualisations, are not affected by the bulges in the middle of the target structures. Furthermore, for the tortuous cylinder, the ACM represents the two relatively sharp turns faithfully.

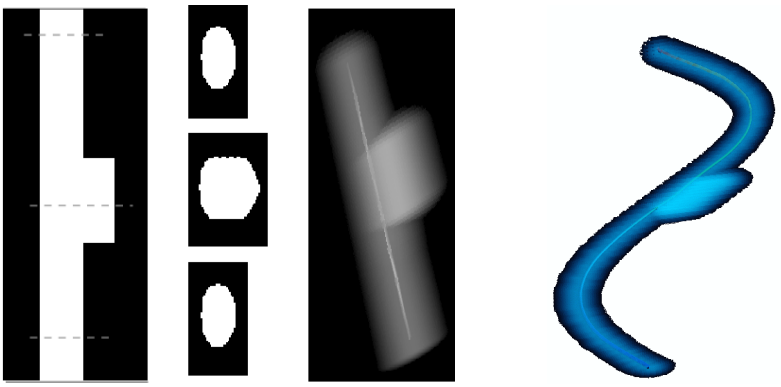

Fig. 1. *Synthetic tubular structures (straight and tortuous) with outside interference: ACMs with 3D visualisations of the tubular structures.*

4.2 Computed Tomography of the Iliac Arteries

Using a Computed Tomography (CT) dataset with a resolution of 512×512×173 ($0.489mm \times 0.489$mm$\times 1.00mm$), we demonstrate the potential of our approach by computing the curvilinear model of the right-hand-side iliac artery (on the left-hand side on an axial slice). In Figures 2 and 3, the top-left or left picture illustrates the spatial relationship between the ACM and the data slice shown. In the other three panels of Figure 2, the ACM of the artery is shown as a white curve penetrating through the axial data slice at three positions separated by a uniform interval of 30 axial slices. In Figure 3, a cronal slice is used instead to allow for assessment from a different angle.

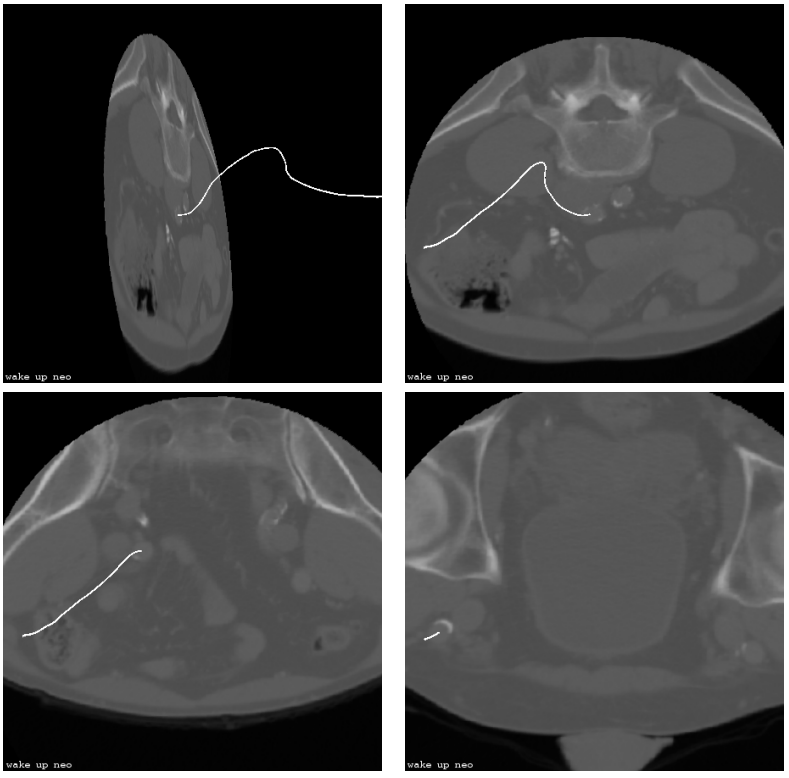

Fig. 2. *ACM of an iliac artery: axial view. Top left: Illustration of* **the spatial relationship** *between the ACM (white curve) and the data slice; Top right and bottom left and right: frontal views at three successive positions along the axial direction, separated by a uniform interval of 30 slices.*

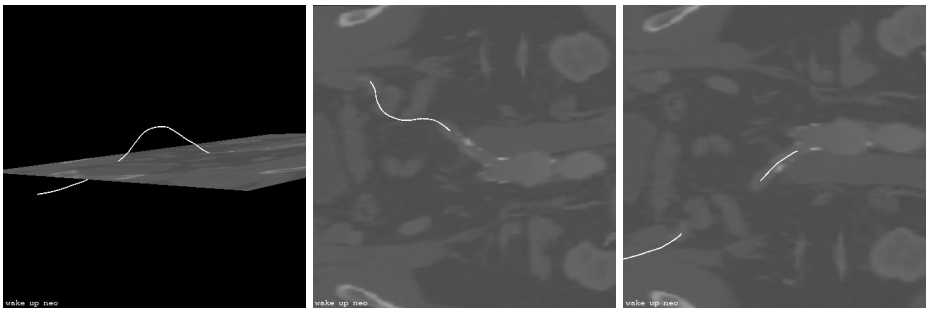

Fig. 3. *ACM of an iliac artery: cronal view. Left: Illustration of the spatial relationship between the ACM (white curve) and the data slice; Middle and Right: front and back views of the ACM and the data as illustrated in the left panel.*

4.3 Magnetic Resonance Angiography of the Carotids

We further illustrate our method using a Magnetic Resonance Angiography (MRA) image with a resolution of 284×512×112 ($0.48mm \times 0.48\text{mm} \times 0.83mm$). Computation of the ACMs of the internal carotids based on such an image can potentially be a prepocessing step for neurosurgery planning. The image and our results are shown in Figure 4. In the left panel, we compare the MCP (dotted line) with the ACM (solid line). In the middle and right panels the ACMs are visualised as curves penetrating the superimposed planes that slice through the MRA data.

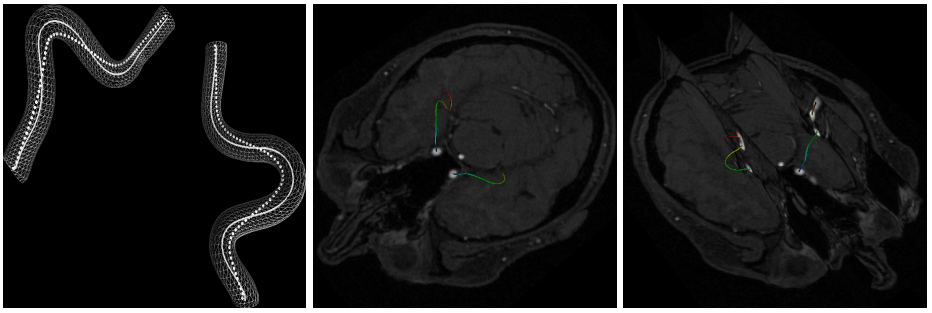

Fig. 4. *ACMs of the internal carotids. Left: comparison of the MCP (dotted line) with the ACM (solid line); Middle and Right: ACMs with superimposed planes that slice through the MRA data.*

5 Discussion and conclusion

In this paper, we have presented an approach for accurate curvilinear modelling, which aims to filter out potential sources of interference in the earliest stages of

processing using *a priori* knowledge. We have demonstrated that this approach is resistant to introducing spurious curvatures (those that are not due to any change in the local orientation of the object of interest), while faithfully reproducing "real" high curvatures (those that are actually part of the object in question).

Acknowledgments The authors would like to thank the University Medical Centre (Utrecht, the Netherlands) and the Neurological Service of Henri Mondor Hospital (Créteil, France) for the clinical data used in this paper.

References

1. D. Adalsteinsson and J.A. Sethian. A fast level set method for propagatong interfaces. *Journal of Computational Physics*, 118:269–277, 1995.
2. S. Aylward and E. Bullitt. Initialization, Noise, Singularities and Scale in Height Ridge Traversal for Tubular Object Centerline Extraction. *IEEE TMI*, 21(2):61–75, 2002.
3. G. Borgefors. Distance transformations in arbitrary dimensions. *Comput. Vision Graphics Image Process*, 27:321–345, 1984.
4. W. A. Brown, R. Miller, S. Birch, and A. Scott. Is aortic angiography necessary for accurate planning of endovascular aortic aneurysm stents? *Cardiovascular Surgery*, 11(1):1–5, 2003.
5. V. Chalana, W. Costa, and Y. Kim. Integrating region growing and edge detection using regularization. In *SPIE*, volume 2434, pages 262–271, 1995.
6. I. Cohen, L. D. Cohen, and Y. Ayache. Using deformable surfaces to segment 3D images and infer differential structures. *CVGIP: Image Understanding*, 56(2):242–263, 1992.
7. L. Cohen and I. Cohen. Finite-Element Methods for Active Contour Models and Balloons for 2-D and 3-D Images. *IEEE PAMI*, 15(11):1131–1147, November 1993.
8. T. Deschamps and L.D. Cohen. Fast extraction of minimal path in 3D images and applications to virtual endoscopy. *Medical Image Analysis*, 5:281–299, 2001.
9. Edsger W. Dijkstra. A note on two problems in connexion with graphs. *Numerische Mathematik*, 1:269–271, 1959.
10. A.F. Frangi, W.J. Niessen, K. Vinken, and M.A. Viergever. Multi-scale vessel enhancement filtering. . In *MICCAI'98*, volume 1496 of *Lecture Notes in Computer Science*, pages 130–137, Cambridge (USA), October 1998. Springer.
11. K. Krissian, G. Malandain, N. Ayache, R. Vaillant, and Y. Trousset. Model-Based Detection of Tubular Structures in 3D Images. *CVIU*, 80:130–171, 2000.
12. R. Li, S. Brown, L. Wilson, J. Young, and S. Luo. Progressively Refined Patient-Specific Vessel System Models from Generic Representations. In *DICTA'02*, pages 184–189, Melbourne, Australia, October 2001.
13. G Lohmann. *Volumetric Image Analysis*. Wiley, 1998.
14. T. McInerney and D. Terzopoulos. Deformable models in medical image analysis: A survey. *Medical Image Analysis*, 1(2):91–108, 1996.
15. N. Nikolaidis and I. Pitas. *3-D Image Processing Algorithms*. John Wiley, 2001.
16. F. Quek and C. Kirbas. Vessel Extraction in Medical Images by Wave Propagation and Traceback. *IEEE Transactions on Medical Imaging*, 20(2):117–131, 2001.

17. Y. Sato, S. Nakajima, N. Shiraga, H. Atsumi, S. Yoshida, T. Koller, G. Gerig, and R. Kikinis. Three-Dimensional Multi-Scale Line Filter for Segmentation and Visualization of Curvilinear Structures in Medical Images. *Medical Image Analysis*, 2(2):143–168, 1998.
18. J.A. Sethian. A fast marching level set method for monotonically advancing fronts. *Proc. of the National Academy of Sciences of the USA*, 93(4):1591–1595, Feb 1996.
19. J.A. Sethian. *Level set methods: Evolving interfaces in geometry, fluid mechanics, computer vision, and materials science.* Number 3 in Cambridge monographs on applied and computational mathematics. Cambridge University Press, 1999.
20. D. Terzopoulos, A. Witkin, and M. Kass. Constraints on deformable models: Recovering 3D shape and nonrigid motion. *Artif. Int.*, 36(1):91–123, 1988.
21. R. Truyen, T. Deschamps, and L.D. Cohen. Clinical Evaluation of an Automatic Path Tracker for Virtual Colonoscopy. In *MICCAI'01*, pages 169–176, Utrecht, The Netherlands, October 2001.
22. O. Wink, W.J. Niessen, and Viergever M. Fast Delineation and Visualization of Vessels in 3-D Angiographic Images. *IEEE TMI*, 19(4):337–346, 2000.
23. P.J. Yim, P.L. Choyke, and R.M. Summers. Gray-Scale Skeletonisation of Small Vessels in Magnetic Resonance Angiography. *IEEE TMI*, 19(6):568–576, 2000.